Journal of Drug Delivery Science and Technology 95 (2024) 105615

Contents lists available at ScienceDirect

Journal of Drug Delivery Science and Technology

journal homepage: www.elsevier.com/locate/jddst

Inhaled nintedanib nanoparticles for enhanced efficacy in idiopathic pulmonary fibrosis (IPF) treatment – Evidence in disease-relevant *in-vitro* models

Xuechun Wang, Mimansa Goyal, Dnyandev Gadhave, Vivek Gupta *

Department of Pharmaceutical Sciences, College of Pharmacy and Health Sciences, St. John's University, 8000 Utopia Parkway, Queens, NY, 11439, USA

ARTICLE INFO

Keywords:
Nintedanib
Idiopathic pulmonary fibrosis
PLGA nanoparticles
Inhalation
Scalable
TGF-β

ABSTRACT

Idiopathic pulmonary fibrosis (IPF) is a fatal and progressive interstitial lung disease with a high mortality rate due to limited prognosis. According to the National Institutes of Health (NIH), approximately 100,000 people in the United States suffer from IPF, and around 50% likelihood of dying within 2–3 years. Currently, nintedanib (Nint) is one of the only 2 FDA-approved drugs for the treatment of IPF, with anti-fibrotic and anti-inflammatory activities. However, Nint oral capsules have some undesirable limitations such as low bioavailability and high dose requirement for sufficient therapeutic efficacy, leading to various side effects associated with oral delivery. To address these shortcomings and enhance the therapeutic potential, Nint was loaded into PLGA nanoparticles (Nint NPs) for localized pulmonary delivery. *In-vitro* cell culture studies indicated that nano-sized particles (179 ± 3 nm) of Nint NPs enhanced cellular uptake in airway epithelial cells and normal human lung fibroblasts, while readily avoiding macrophage phagocytosis. Transforming growth factor-beta (TGF-β) (10 ng/mL) was selected to establish IPF in cells, which resulted in proliferation and rapid wound healing, whereas Nint NPs showed superior ability in inhibiting these pathological phenomena compared to free Nint. Upon further evaluation of pathological mechanisms of IPF, Nint NPs remarkably attenuated epithelial-to-mesenchymal transition (EMT) by elevating epithelial marker E-cadherin level and reducing extracellular matrix (ECM) deposition by evidence of reduced collagen production and fibroblast-to-myofibroblast differentiation marker, α-SMA. Nint NPs also decreased expression of inflammatory cytokine IL-17A and indicated autophagy as a separate anti-fibrotic mechanism. Finally, Nint NPs proved their superior efficacy in a novel IPF cell model using diseased lung ECM substrates. Hence, inhalation therapy of Nint NPs is a promising alternative tool for oral capsules in IPF therapy.

1. Introduction

Pulmonary fibrosis (PF) is a form of interstitial lung disease that involves the gradual and widespread restructuring of lung tissue, resulting in the deposition of extracellular matrix (ECM) and permanent scarring [1,2]. Currently, idiopathic pulmonary fibrosis (IPF) stands as the prevailing and most severe form of PF with a median life expectancy of 3–5 years after diagnosis [3]. IPF is considered a rare disease that typically impacts individuals aged 50–70 years. As per the National Institute of Health (NIH), about 100,000 people in the United States are affected by IPF, and approximately 30,000 to 40,000 new cases are diagnosed annually. Globally, the prevalence of IPF is estimated to be between 13 and 20 cases per 100,000 individuals [4]. Presently it is believed that the persistent damage to the alveolar epithelium leads to unregulated growth of Type-II alveolar epithelial cells and epithelial-to-mesenchymal transition (EMT), which further release numerous fibrogenic growth factors and cytokines such as transforming growth factor-beta (TGF-β), fibroblast growth factor (FGF), platelet-derived growth factor (PDGF), interleukins, and vascular endothelial growth factor (VEGF), that initiate pro-fibrotic and inflammatory signaling cascades, once bound to their respective surface receptors [5–7]. Consequently, activated fibroblasts undergo transformation into myofibroblasts, which play a crucial role in the excessive production of ECM components, and thickening and stiffening of the lung tissues [8].

In 2014, oral nintedanib (Nint) (brand name: Ofev®) was one of the first 2 medications approved by the FDA for IPF treatment (Pirfenidone

* Corresponding author. College of Pharmacy and Health Sciences, St. John's University, 8000 Utopia Parkway, Queens, NY, 11439, USA.
E-mail address: guptav@stjohns.edu (V. Gupta).

https://doi.org/10.1016/j.jddst.2024.105615
Received 10 December 2023; Received in revised form 22 March 2024; Accepted 24 March 2024
Available online 26 March 2024

Abbreviations

α-SMA	α-smooth muscle actin
%DL	% drug loading
%EE	% entrapment efficiency
AEC	primary airway epithelial cells
COL1A1	human pro-collagen I alpha 1
DCM	dichloromethane
DMSO	dimethyl sulfoxide
ECM	extracellular matrix
ELISA	enzyme-linked immunosorbent assay
EMT	epithelial-to-mesenchymal transition
FGF	fibroblast growth factor
HPH	high pressure homogenization
IL-17	interleukin-17
IPF	idiopathic pulmonary fibrosis
MTT	3-(4,5-dimethylthiazol-2-yl)-2,5-diphenyltetrazolium bromide
NHLF	normal human lung fibroblasts
Nint	nintedanib
Nint NP	nintedanib nanoparticles
NSCLC	non-small-cell lung cancer
PDGF	platelet-derived growth factor
PDI	polydispersity
PLGA	poly(D,L-lactide-co-glycolide 50:50)
PS	particle size
PVA	poly vinyl alcohol
TGF-β	transforming growth factor-beta
VEGF	vascular endothelial growth factor

being the other one) [9]. Nint, a small-molecule triple-tyrosine kinase inhibitor, acts by competitively obstructing the adenosine triphosphate binding sites of both receptor tyrosine kinases and non-receptor tyrosine kinases, including PDGFR, FGFR, and VEGFR [10]. Inhibition of these kinase activities exerts therapeutic actions by interrupting cellular processes leading to lung fibrosis [11,12]. Based on clinical data, while the highest oral dose of Nint (150 mg twice a day) significantly slows down the progression of IPF, it also leads to notable adverse effects such as diarrhea, liver injury, and nausea [9,13,14]. Due to associated safety concerns, increasing the dosage of oral Nint for potentially enhanced efficacy is not a viable option [14]. On the pharmacokinetic side, Nint oral capsule displays extremely limited bioavailability (<5%) due to substantial P-glycoprotein (P-gp) efflux, extensive first-pass metabolism, and low aqueous solubility [10]. Due to these delivery route-associated shortcomings, lungs' exposure to Nint is extremely limited, resulting in moderate efficacy. Taken together, there is an urgent need for more exploration to develop targeted Nint treatments for prolonging life and improving quality of life for IPF patients.

Recently, inhalation has demonstrated tremendous potential as a local route of delivery for the treatment of respiratory diseases. Pulmonary route of administration permits localized lung delivery and largely bypasses the gastrointestinal tract and first-pass metabolism, thus effectively circumventing oral delivery-associated side effects [15]. Moreover, much reduced dose is required for direct-to-lung delivery due to targeted lung administration as well as the flexibility of increasing the dosage to enhance the effectiveness of IPF treatment while ensuring it remains below the safety threshold associated with oral administration. The potential of inhaled Nint was studied in two recent publications in 2020 [9,15]. Both studies formulated Nint into solutions containing low percentages (1.5–2%) of propylene glycol to solubilize the drug. In one of the studies, Nint pharmacokinetics following oral (60 mg/kg) and inhaled (0.5 and 0.1 mg/kg) administration showed that inhaled Nint was able to achieve oral-equivalent lung C_{max} with substantially lower systemic exposure [9]. Both studies indicated flip-flop pharmacokinetics of oral Nint, meaning Nint eliminated faster than it can accumulate in plasma. This phenomenon is the result of a combination of significant Nint tissue partitioning and rapid metabolism. In other words, while intestinal absorption is rapidly occurring, however, first-pass metabolism and rapid Nint tissue partitioning result in low plasma levels that do not accurately reflect oral bioavailability or systemic exposure [9,15]. Furthermore, inhaled dose also led to weight gain in bleomycin-challenged animals equivalent to that of the control group. In contrast, oral administration resulted in substantially lower weight gain than the control group, indicating a negative health effect on animals undergoing fibrosis and receiving oral Nint [9]. In the efficacy studies using animal IPF models, inhalation was well-tolerated and effective in diminishing inflammatory and fibrotic markers, however, oral-superior pulmonary efficacy was not consistently demonstrated [9,15]. Therefore, in an attempt to further improve the efficacy of inhaled Nint, we recently formulated Nint into inhalable poly(lactic-co-glycolic acid) (PLGA) nanoparticles for IPF treatment [16]. Nanoparticles are known for their enhanced cellular uptake; and their small particle sizes (<200 nm) are small enough to avoid recognition thus escaping detection by alveolar macrophages [17]. Various inhalable PLGA-based nanoparticles have been reported the enhanced treatment of IPF. For instance, inhalation of simvastatin (SV)-loaded PLGA nanoparticles was shown to significantly prevent progression of paraquat-induced PF in rats through reducing plasma concentration of inflammatory factors as well as contractile responses. Whereas, inhalation of plain SV could not avert fibrosis and tissue damage [18].

In our recent publication, inhalable Nint NPs formulation was optimized using the scalable high-pressure homogenization (HPH) technique which resulted in reproducible small particle sizes (<200 nm), mono-dispersity, and excellent stability [16]. Nint NPs also demonstrated excellent aerodynamic behavior suggesting feasibility for pulmonary route of administration for deep lung deposition. The aim of the present study is to address the shortcomings of Nint and maximize its potential for the treatment of IPF, by using inhaled Nint-Loaded NPs. The anti-fibrotic and anti-inflammatory activities of Nint NPs as well as other mechanism of actions are elucidated using two *in-vitro* cell models of IPF, including a disease-relevant IPF model.

2. Materials and methods

2.1. Materials

Nintedanib, Free base (Nint) was purchased from LC Laboratories (Woburn, MA, USA). Resomer® RG 502H (Poly (D, L-lactide-co-glycolide 50:50) (PLGA; MW 7,000-17,000 Da) was acquired from Evonik (Parsippany, NJ, USA). Poly vinyl alcohol (PVA), and TGF-β1 (Human Recombinant Animal Free transforming growth factor beta) were purchased from Sigma-Aldrich (St. Louis, MO, USA). 3-(4,5-dimethylthiazol-2-yl)-2,5-diphenyltetrazolium bromide (MTT), dichloromethane (DCM), dimethyl sulfoxide (DMSO), HPLC/LC-MS grade methanol, acetonitrile (ACN) and water were purchased from Fisher Scientific (Hampton, NH, USA). Other assay kits and molecular biology grade reagents were obtained from other commercial vendors which are listed at appropriate places throughout the manuscript.

Non-small-cell-lung-cancer (NSCLC) cell line A549 was acquired from ATCC (Manassas, VA, USA) and maintained in RPMI 1640 medium (Corning) supplemented with 10% FBS (Atlanta Biologicals), sodium pyruvate, and penicillin-streptomycin. Primary airway epithelial cells (AEC) were obtained from ATCC (Manassas, VA, USA) and maintained in airway epithelial cell basal medium supplemented with

corresponding bronchial epithelial cell growth kit (ATCC, Manassas, VA, USA). Normal human lung fibroblasts (NHLF) were purchased from Lonza (Walkersville, MD, USA) and maintained in FBM™ Basal medium and FGM™-2 SingleQuots supplements (Lonza, Walkersville, MD, USA). All cell lines were incubated at 37 °C/5% CO_2 and 90-100% relative humidity.

2.2. Formulation and characterization of inhalable Nint-Loaded PLGA nanoparticles

Nint-Loaded PLGA nanoparticles were developed and characterized as illustrated in our recently published study [16]. NH9, the optimized Nint-Loaded nanoparticle formulation in earlier study was formulated, and characterized for particle size, zeta potential, polydispersity, drug content and release, inhalability, stability, intracellular uptake, and *in-vitro* safety. The UPLC method and equations used to calculate % entrapment efficiency (%EE) and % drug loading (%DL) are provided in *Supplementary Information.* A brief preparation method is provided below, and summary characterization data is presented in *Supplementary Information* **(**Table S1**)** [16].

Optimized Nint NPs were fabricated using high pressure homogenization (HPH), following a recently published protocol [16]. Briefly, coarse emulsion of organic phase (Nint + PLGA in dichloromethane) and aqueous phase (1% w/v PVA solution in water) was prepared by homogenization (3 min at 10,000 rpm). Coarse emulsion was processed through HPH (Nano DeBee; BEE International, South Easton, MA, USA) at a pressure of 25,000 psi with no recirculation of the formulation. Z5 nozzle with a diameter of 13 mm was selected to pass the non-viscous formulation. The final emulsion was stirred overnight to remove the organic solvent. Next day, larger particles and unencapsulated drug were removed by centrifugation at 3,000 rpm for 3 min. The supernatant containing nanoparticles were further washed twice using Milli-Q water by centrifugation at 21,000×*g* for 15 min to remove any unentrapped drug/polymer. Final formulation was reconstituted in 1 mL of water; and was used for further studies as described in earlier study [16].

2.3. TGF-β induced proliferation assay

Prior to performing proliferation assays, a preliminary 48 h cell viability study was performed to determine a suitable Nint concentration for IPF treatment, using MTT assay as described in our previous publications [19]. According to the finding of the cell viability studies, Nint concentrations up to 3.125 μM were used for proliferation assays.

Proliferation studies were carried out on A549, primary airway epithelial cells (AEC), and normal human lung fibroblasts (NHLF) cell lines. Human Recombinant Transforming growth factor-Beta (TGF-β) was used to induce IPF disease model in all the cells tested. Briefly, 2,500 cells/well were plated in 96-well plates followed by 24 h of serum starvation (using serum-free media). Then cells were treated with TGF-β (10 ng/mL) and varying concentrations of Nint and Nint NPs (0.625, 1.25, and 2.5 μM) for 48 h. Serum-free media acted as control. Cell proliferation was analyzed by performing the MTT assay, as described before.

2.4. TGF-β-induced epithelial-to-mesenchymal transition (EMT)

EMT is a major event in IPF pathogenesis that contributes to development of migratory and invasive properties in diseased cells [8,20]. To visualize the EMT phenomenon, a phenotypic study was completed. In brief, AEC cells were plated on 24-well plates at a cell density of 8.0×10^4 cells/well, followed by 24 h serum-starvation. Afterwards, cells were treated with TGF-β (10 ng/mL) in the presence and absence of Nint and Nint NP (1.25 and 2.5 μM equivalent) for 48 h. Cell images were taken using EVOS FL fluorescence microscope (Thermo Fisher Scientific, Waltham, MA, USA) at 10x magnification on transmission setting, and were analyzed for changes in cellular morphology.

2.5. E-cadherin (E-cad) quantification

E-cadherin is an essential protein present on epithelial cells that plays a vital role in facilitating cell-cell adhesion. This protein helps maintain the integrity of epithelial cells, inhibiting their migration and proliferation [21]. The suppression of E-cadherin expression induces mesenchymal features or EMT, the main pathogenic driver in IPF cell motility and invasion [22]. The concentration of E-cadherin (soluble E-cadherin) in supernatants of cell culture were quantified using Human E-cadherin Quantikine ELISA kit (R&D Systems, Inc., Minneapolis, MN, USA). All ELISA assays used in this project employed the quantitative sandwich enzyme immunoassay technique, in which the specific monoclonal antibody has been pre-coated onto a microplate. Briefly, AEC cells were seeded at 1×10^5 cells/well in a 24-well plate, followed by 24 h serum-starvation. Cells were stimulated with TGF-β (10 ng/mL) in the presence and absence of Nint and Nint NP (0.625, 1.25, and 2.5 μM equivalent). After 48 h, the cell culture supernatant was centrifuged at a speed of 5,000 rpm for 5 min at 4 °C. Samples were examined using ELISA following the manufacturer's instructions to quantify the amounts of soluble E-Cad in the samples. Absorbance at 450 nm was read and corrected with 540 nm reading using Spark 10 M Plate Reader. The concentration of E-cadherin was quantified against a standard curve.

2.6. Cell migration assay

Cell migration assay or wound healing assay was conducted according to a previous publication [23]. AEC and NHLF cells were seeded in 24-well plates at a cell density of 1×10^5 cells/well, followed by 24 h serum-starvation, after which, scratches were made in each well using a 200 μL microtip. Cells were stimulated with TGF-β (10 ng/mL) in the presence and absence of Nint and Nint NP (1.25 and 2.5 μM equivalent). Migration of cells from edges were monitored at 0, 24, and 48 h. Images were taken using an inverted microscope (Laxco, Mill Creek, WA, USA) at 10x objective. Scratch widths were measured using ImageJ Software (National Institute of Health, USA) to calculate % of the scratch closure against no-treatment control.

2.7. Identification and measurement of fibrillar collagens

The collagen content in NHLF cells was measured with the Sirius red/fast green collagen staining kit (Chondrex Inc., Redmond, USA) following a previous report [23]. The study was separated into two parts: qualitative imaging and quantitative detection. For imaging study, NHLF cells seeded at a density of 5.0×10^4 cells/well in 24-well plates were serum starved for 24 h and subsequently stimulated with TGF-β (10 ng/mL) in the presence and absence of Nint and Nint NP (1.25 and 2.5 μM equivalent). After 48 h, cells were washed with PBS (pH 7.4) and fixed with 4% paraformaldehyde for 10 min. Fixed cells were washed with PBS and incubated with dye solution for 30 min at room temperature. After staining, cells were washed with distilled water until the water runs clear. Cells were immediately imaged using an inverted microscope (Laxco, Mill Creek, WA, USA) at 10x objective. On the other hand, quantitative analysis was done by seeding 2,500 cells/well in 96-well plates. The treatments and procedure follow the same as qualitative study. After washing the cells of the dye, staining was extracted using extraction buffer. Optical density of the extracted solutions was determined at 540 nm and 605 nm using Spark 10 M Plate Reader. The collagen content of each group was determined by the following equation (Eq. 1):

$$Collagen\left(\frac{\mu g}{section}\right) = \frac{OD\ 540\ value - (OD\ 605\ value * 0.291)}{0.0378} \quad (1)$$

2.8. Western blot assessment of α-Smooth muscle actin expression (α-SMA)

This study employed a pre-existing western blotting protocol [24]. Briefly, NHLF cells were plated at 5.0 × 10^5 cells per 100 mm tissue culture dishes followed by 24 h serum starvation. The cells were treated with TGF-β (10 ng/mL) in the presence and absence of Nint and Nint NP (1.25 and 2.5 μM equivalent). After 48 h, the cells were harvested and lysed using a solution of 1% Triton® X-100 (Fisher Scientific, Waltham, MA, USA), 1% Halt™ Protease and Phosphatase Inhibitor Cocktail (Thermo Fisher Scientific, Waltham, MA, USA) in PBS. The lysates were then sonicated for 1 h at 4 °C. Following sonication, the samples were centrifuged at 15,000 rpm for 15 min at 4 °C to collect the lysates. The protein content of the lysates was quantified using the DC™ Protein Assay Kit (Bio-Rad, Hercules, CA, USA). Subsequently, the samples were mixed with 2x Laemmli buffer (Bio-Rad, Hercules, CA, USA) and 2-mercaptoethanol, and denatured at 100 °C for 10 min. Bovine serum albumin (BSA) content of each sample was calculated and diluted with PBS to normalize BSA content. Then 12 μL samples were loaded on 4-20% Mini-PROTEAN® TGXTM Precast Protein Gels (Bio-Rad) and transferred on Trans-Blot® Turbo™ Midi PVDF membranes (Bio-Rad) using a Bio-Rad PowerPac™ Basic Power Supply and Trans-Blot® Turbo™ system. The membranes were blocked with 5% BSA in PBS and then spiked with α-SMA (#19245S) and GAPDH (#5174S) (Cell Signaling Technology, Danvers, MA, USA) (1:1000 dilution) and kept for overnight shaking at 4 °C. Next day, membranes were incubated with corresponding secondary HRP-conjugated antibody goat anti-rabbit (#32260) (Thermo Fisher Scientific, Waltham, MA, USA) (1:10,000 dilution) for 2 h at room temperature and subjected to Western Bright chemiluminescence (WBF25, The Gel Company, San Francisco, CA, USA). Protein signals were detected on the membrane and were quantified using chemiluminescent imaging by the Omega Lum™ G Imaging System (The Gel Company, San Francisco, CA, USA). Densitometry for all protein bands was performed using ImageJ software ver. 2.0.

2.9. Interleukin-17 (IL-17) ELISA

The concentration of human IL-17 in supernatants of cell culture were measured using Human IL-17 ELISA kit (R&D Systems, Minneapolis, MN, USA). NHLF cells were seeded and treated in the same manner as described in **Section 2.8**. After 48 h, the cell culture supernatant was centrifuged at a speed of 5,000 rpm for 5 min at 4 °C. Samples were immediately examined for IL-17 quantification following the manufacturer's instructions. Absorbance at 450 nm was read and corrected using the 540 nm reading using Spark 10 M Plate Reader. The concentration of IL-17 was quantified against a standard curve.

2.10. Effect of Nint and Nint NP on cellular autophagy

CYTO-ID® Autophagy Detection Kit (Enzo Life Sciences, Farmingdale, NY, USA) was utilized to assess the impact of Nint and Nint NP on autophagy in NHLF cells, by following a published protocol [25]. NHLF cells were seeded in 96-well plates at a density of 25,000 cells/-well and subjected to serum-free media for 24 h to induce autophagy linked to starvation. Subsequently, cells were treated with TGF-β (10 ng/mL) in the presence or absence of Nint and Nint NP (equivalent to 1.25 and 2.5 μM) for an additional 18 h. The treatments were then replaced with 1X assay buffer (100 μL), and a dual color detection reagent was added, followed by incubation in the dark at 37 °C for 30 min. The dual color detection reagent consisted of CYTO-ID® Green Detection Reagent and Hoechst 33,342 nuclear stain in growth medium without phenol red indicator supplemented with 5% FBS. After incubation, the excess dye was removed by washing with 1X assay buffer, and 100 μL of 1X assay buffer was added to each well. CYTO-ID® Green Detection Reagent was read using a FITC filter (480 nm/530 nm ex/em), and the Hoechst 33,342 Nuclear Stain was read using a DAPI filter set (340 nm/480 nm ex/em) in a Spark 10 M plate reader.

2.11. Development of a biorelevant cell-based in-vitro model of IPF

A novel IPF cell model was established using 2D Human Disease NativeCoat™ Lung ECM Surface Coating Kit (Xylyx Bio, Brooklyn, New York, USA). The coating comprised of extracellular matrix (ECM) components isolated from fibrotic human lungs that recapitulated the human IPF disease environment *in-vitro* [26]. Before seeding the cells, the NativeCoat™ ECM surface coating solution was prepared according to manufacturer instructions to a final concentration of 0.2 mg/mL 30 μL of surface coating were added to each well in 96-well plates. The multi-well plates were gently swirled for 30 s to ensure even coating followed by incubation at 37 °C for 2 h. The NativeCoat™ IPF lung ECM-derived plates were utilized for 2 efficacy studies for Nint NPs: proliferation studies and collagen accumulation studies.

2.11.1. Proliferation study

For proliferation study, after 2 h incubation, surface coating was aspirated. Each cell culture surface was washed with 1x PBS and then NHLF cells were seeded at a density of 2,500 cells/well. 1 Day after seeding the cells, they were serum-starved for 24 h followed by Nint and Nint NP treatments, as described earlier, with the same concentrations used as in the TGF-β induced proliferation studies (0.625, 1.25, and 2.5 μM). No TGF-β induction was used for these studies since the diseased surface coating was the biorelevant alternative to induce IPF environment. Other study conditions for the proliferation assay are kept consistent with the ones described in **Section 2.3**.

2.11.2. Human pro-collagen I alpha 1 (COL1A1) ELISA

The second study used Human COL1A1 ELISA kit (Ray Biotech Life, Inc., Peachtree Corners, GA, USA) for the quantitative measurement of COL1A1. The coating step was same as above, however, since 24-well plates were used for this study, 300 μL of the surface coating was used to coat the cell culture surface. NHLF cells were seeded at 1 × 10^5 cells/well in a 24-well plate, followed by 24 h serum-starvation. Cells were then treated in the presence and absence of Nint and Nint NP (1.25, and 2.5 μM equivalent). After 48 h, the cell culture supernatant was centrifuged at a speed of 5,000 rpm for 5 min at 4 °C. Samples were used for human COL1A1 quantification following the manufacturer's instructions. Absorbance at 450 nm was read using Spark 10 M Plate Reader. Concentrations of COL1A1 were calculated against a standard curve.

2.12. Statistical analysis and data presentation

Unless stated otherwise, all the results are reported as mean ± SD or SEM. Unpaired student's t-test was employed for comparing two groups, while one-way analysis of variance (ANOVA) followed by Tukey's multiple comparisons test was used to compare more than two groups. GraphPad Prism software (Version 7.04 for Windows, GraphPad Software, San Diego, California USA) was utilized for statistical analysis. *P* values <0.05 was considered statistically significant. In certain instances, a smaller *p*-value of 0.01 or less, when applicable, is reported.

3. Results

3.1. Characterizations of nint NPs

UPLC was used to calculate %EE, and as shown in Table S1, Nint NPs possessed a high %EE of 43.3 ± 4.0% (equivalent to 2,067.3 ± 467.5 μg/mL of Nint) or %DL of 3.3 ± 0.8%. The HPH method produced particles of small geometric size of 179 ± 3 nm as well as low PDI of 0.186 ± 0.1, which is an indication of mono-dispersibility. Nint NPs possessed stable zeta potential of −23.4 ± 1.9 mV.

3.2. TGF-β induced cellular proliferation

To determine whether Nint could ameliorate growth factor-induced cellular hyper-proliferation, one of the salient features of pulmonary fibrosis *in-vitro*, A549 cells were treated with 10 ng/mL TGF-β for 48 h to induce proliferation. Cell viability of treated cells in addition to Nint from 1.56 to 50 μM is demonstrated in Fig. 1A. At higher concentrations (25 and 50 μM), Nint led significant cytotoxicity, as represented by <20% cell viability. Concentrations below 6.25 μM showed negligible toxicity that is comparable to the negative control group, hence, a Nint concentration of less than 3.125 μM was chosen for all further *in-vitro* cell culturing models.

Next, various concentrations (0.625, 1.25, and 2.5 μM) of Nint and Nint NPs were tested to evaluate the efficacy of the Nint-encapsulated nanoparticle formulation. Proliferation studies were performed on TGF-β-induced A549 cells as well as on AEC and NHLF cells to reflect a more realistic IPF cell model. A shown in Fig. 1B and C, TGF-β-treated cells resulted in significant increase in proliferation in all three cell lines (1.2–1.9-fold increase in cell growth compared to control; $p < 0.05$). Nint and Nint NPs suppressed proliferation in a dose-dependent manner, with nanoparticles consistently showing more suppression compared to Nint at each concentration. In Fig. 1B, Nint NPs significantly reduced proliferation compared to Nint at each concentration tested and TGF-β group ($p < 0.05$). The results on AEC or NHLF cells were not as significant as found on A549 cells. While no significant differences were found between Nint and formulation, Nint NP showed significant reduction in proliferation compared to TGF-β group at each concentration on AEC cells ($p < 0.01$ and $p < 0.001$) (Fig. 1C). Whereas only the highest concentration (2.5 μM) of free Nint showed significant reduction in proliferation compared to TGF-β group ($p < 0.01$). With NHLF cells, statistical significance was found between Nint and formulation at 0.625 μM ($p < 0.01$) and each Nint NP group with TGF-β group ($p < 0.01$, $p < 0.001$, *and* $p < 0.0001$, respective to increasing concentrations) (Fig. 1D). For all 3 cell lines, Nint NP groups were more effective in reducing cellular proliferation to the level of untreated control, which justifies their higher efficacy compared to plain Nint. Preliminary data suggest the superiority of Nint NP at suppressing TGF-β-induced proliferation.

3.3. TGF-β-induced epithelial-to-mesenchymal (EMT) transition

In normal physiology, human airway epithelial cells (AEC) exhibit a cobblestone-like shape. However, when the cells undergo EMT process, a cornerstone of IPF development, AECs would demonstrate an elongated spindle-shaped mesenchymal phenotype. Treatment with growth factors including TGF-β has been shown to induce EMT process in epithelial cells. EMT is also characterized by the loss of cell-cell adhesion, as noticed by increased space between individual cells [27,28]. As can be seen in Fig. 2A, AEC cells converted into elongated spindle-shaped mesenchymal phenotype following treatment with TGF-β (10 ng/ml) (Fig. 2A). At both concentrations tested (1.25 and 2.5 μM), Nint NPs were much better at inhibiting morphological change as compared to free Nint. Cells incubated with 2.5 μM of Nint NPs showed very similar morphology as control cells, whereas Nint at 2.5 μM showed a mix of epithelial and mesenchymal phenotypes.

3.4. E-cadherin (E-cad) expression in epithelial cells

Epithelial Cadherin (E-Cadherin; E-Cad) is a protein that is vital for cell adhesion and for maintaining epithelial phenotype of the cells. E-

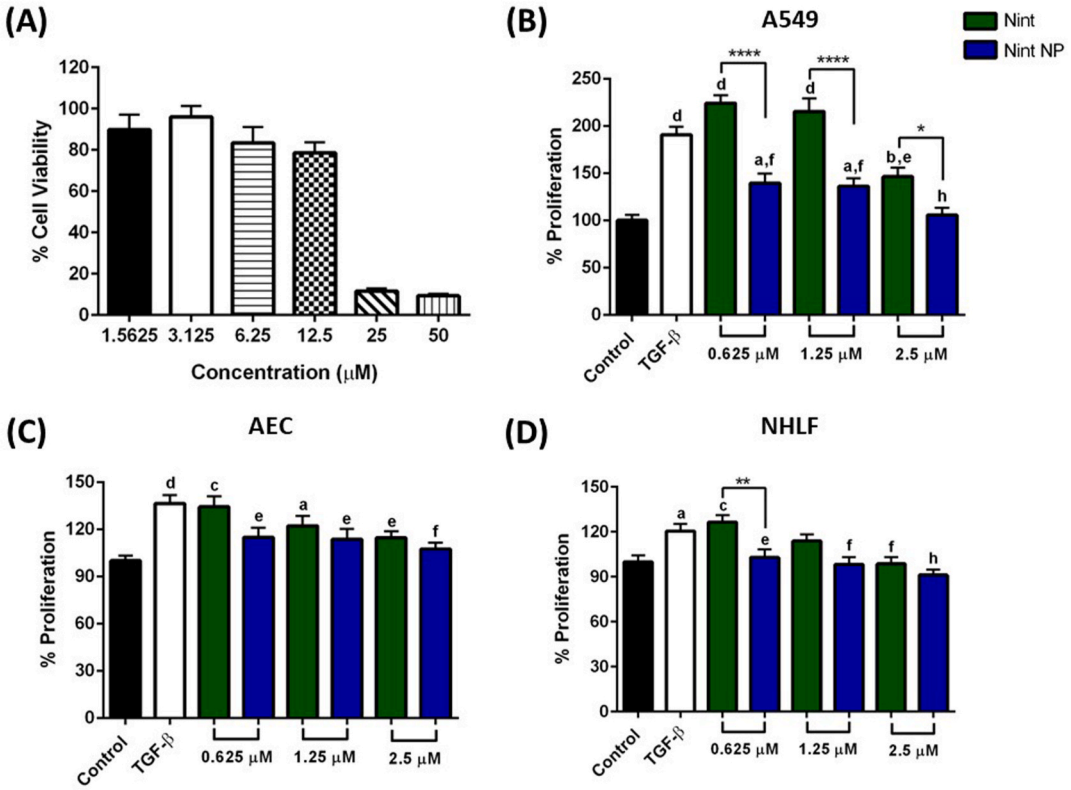

Fig. 1. A. Cytotoxicity of Nint against A549 cells to determine the concentration for IPF treatment. Cells were treated with TGF-β (10 ng/mL) and various concentrations of Nint (following 24 h starvation) for 48 h and cell viability was measured using MTT assay. Data represent mean ± SD (n = 6). Proliferation studies of Nint vs. Nint NPs on **B.** A549, **C.** AEC, and **D.** NHLF cells. After 24 h serum starvation, cells were treated with TGF-β (10 ng/mL) in the presence or absence of Nint and Nint NPs for 48 h $*p < 0.05$, $**p < 0.01$, and $****p < 0.0001$ comparisons between Nint and Nint NP. $a < 0.05$, $b < 0.01$, $c < 0.001$, and $d < 0.0001$ compared to control. $e < 0.05$, $f < 0.01$, and $h < 0.0001$ compared to TGF-β. Data represent mean ± SEM of three separate trials each with n = 6.

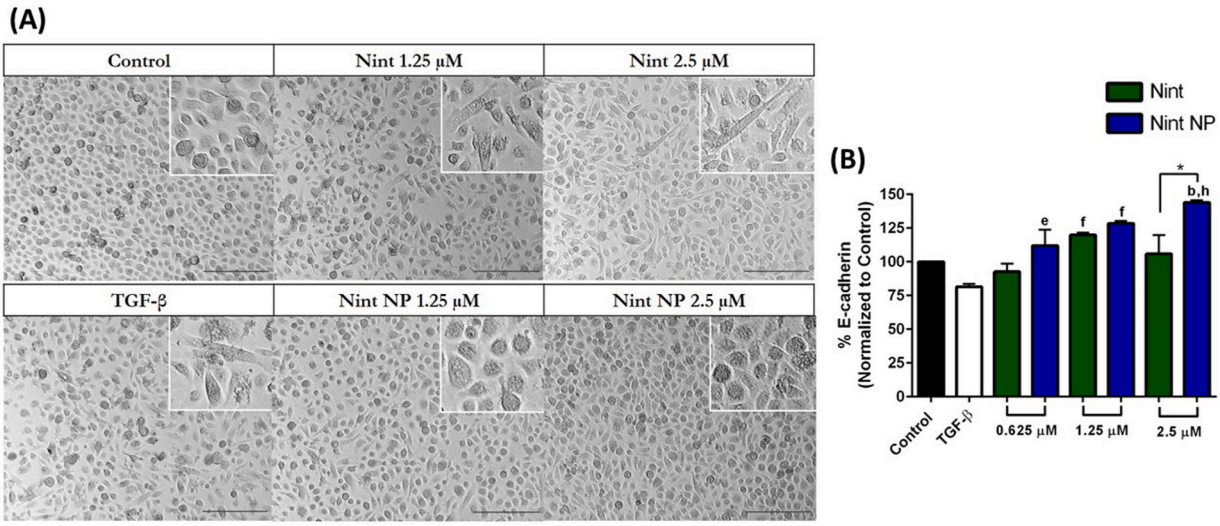

Fig. 2. TGF-β induces EMT-associated phenotypic alterations in AEC cells. **A.** Representative images were taken at 10x magnification of AEC cells (serum-starved for 24 h) cultured with TGF-β (10 ng/mL) in the presence or absence of Nint and Nint NPs after 48 h. Cells grown in serum-free media were considered as control. Scale bar = 100 μm. **B.** Quantification of soluble E-cadherin levels in media supernatants of AEC cells using ELISA method. $*p < 0.05$ comparisons between Nint and Nint NP. $b < 0.01$ compared to control. $e < 0.05$, $f < 0.01$, and $h < 0.0001$ compared to TGF-β. Data represent mean ± SEM (n = 3).

cad expression is a very sensitive biomarker for EMT progression, as E-cad levels are downregulated by the EMT progression, resulting in loss of cell-cell adhesion and tight junctions [29]. We determined soluble E-cadherin levels in cell culture supernatant using the ELISA method. As seen in Fig. 2B, TGF-β (10 ng/ml) treatment suppressed the E-cadherin levels compared to control (81.5 ± 2.0%), where Nint and Nint NPs treatment prevented that reduction. Nint NP treatment at a low concentration of 0.625 μM, restored E-cad expression in cells (112.1 ± 11.7%, $p < 0.05$ compared to TGF-β group), whereas Nint (92.7 ± 6.0%) showed no significant increase in E-cad expression. Nint NPs

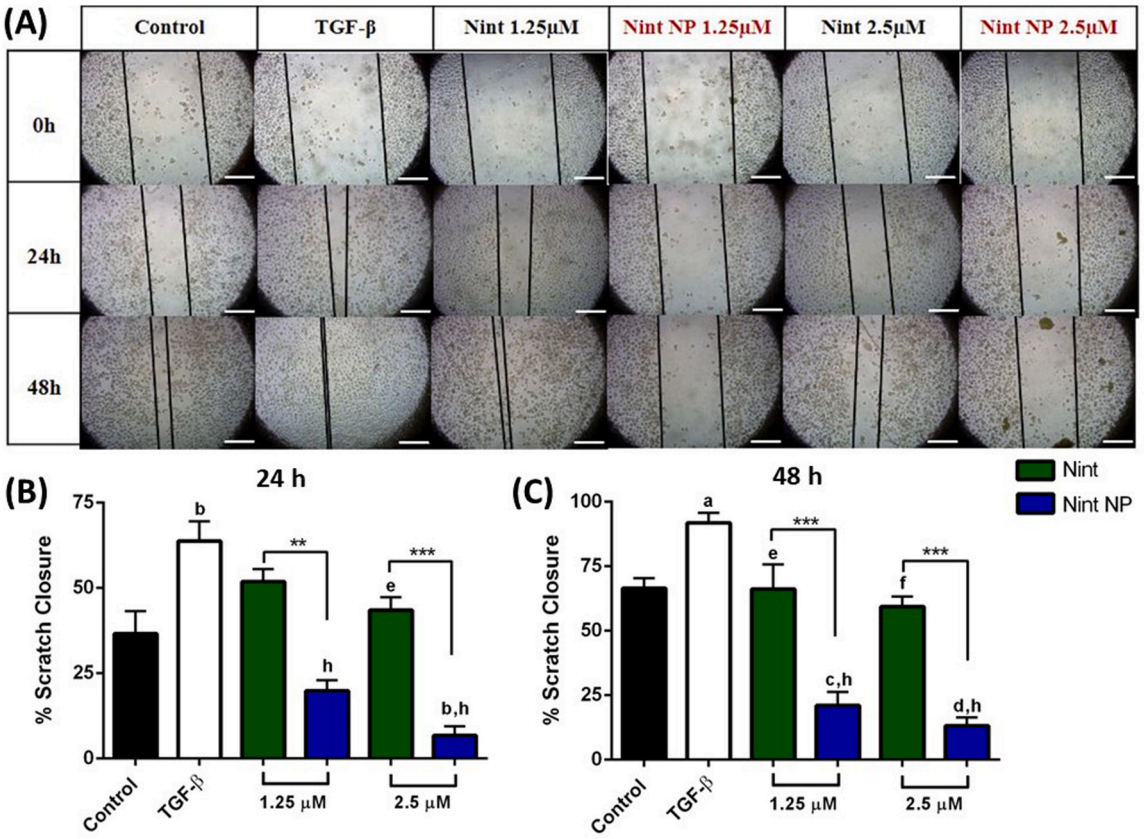

Fig. 3. *In-vitro* wound healing assay with AEC cells. On confluent serum-starved AEC cell monolayer, a scratch was created followed by treatment with TGF-β (10 ng/mL) in the presence or absence of Nint and Nint NPs. **A.** Representative images were taken at 10x objective after 24 and 48 h treatment. Cell migration quantification as % scratch closure at **B.** 24 h and **C.** 48 h. $**p < 0.01$ and $*** p < 0.001$ comparisons between Nint and Nint NP. $a < 0.05$, $b < 0.01$, $c < 0.001$, and $d < 0.0001$ compared to control. $e < 0.05$, $f < 0.01$, and $h < 0.0001$ compared to TGF-β. Data represent mean ± SEM (n = 3). Scale bar = 500 μm.

significantly increased E-cadherin levels compared to TGF-β group at all tested concentrations ($p < 0.05$, $p < 0.01$, and $p < 0.0001$ respective to increasing concentrations). At 1.25 μM, both Nint (119.9 ± 1.6%) and Nint NP (128.5 ± 1.8%) significantly increased E-cad levels compared to TGF-β group ($p < 0.01$). Treatments at 2.5 μM showed Nint NP significantly increased E-cad expression compared to Nint (Nint: 105.9 ± 13.9%; Nint NP: 144.0 ± 1.7 %) ($p < 0.05$) and control groups ($p < 0.01$ compared to control, $p < 0.0001$ compared to TGF-β group).

3.5. Cell migration assay

One of the consequences of overexpressed TGF-β and reduced E-cadherin expression in cells is the increase of cell motility that aggravates fibrosis. Therefore, a scratch (or wound healing) assay was done to evaluate whether the addition of Nint or Nint NP can inhibit the migratory ability of TGF-β-induced cells, by quantifying scratch closure over time in a monolayer of cells. Figs. 3A and 4A show representative images of wounds created by scratching serum-starved cells with a sterile 200 μL microtip, followed by Nint/Nint-NP treatments for 24 and 48 h. Results of the study depicted that TGF-β stimulation demonstrated faster migration of cells, resulting in complete wound closure after 48 h, whereas co-treatment with Nint and Nint NP significantly reduced/blocked cellular migration. Quantifications of % scratch closures are displayed in Fig. 3B & **C (AEC)** and Fig. 4B & **C (NHLF)**, where both treatments suppressed scratch closure in a dose-dependent manner, with nanoparticles found to be significantly more potent than free Nint. For example, AEC wound closure after 24h for 2.5 μM equivalent of Nint and Nint NP was 43.5 ± 3.7% and 6.7 ± 2.7%, respectively ($p < 0.001$), and after 48h was 59.2 ± 3.9% and 13.0 ± 3.2%, respectively ($p < 0.001$). At the same time, NHLF wound closure after 24h for 2.5 μM equivalent of Nint and Nint NP was 28.5 ± 6.7% and 9.5 ± 1.9%, respectively, and after 48h was 44.1 ± 4.4 % and 13.9 ± 2.7%, respectively ($p < 0.001$).

3.6. Effects on collagen production in fibroblasts

One explanation of excessive production of fibroblasts and myofibroblasts is due to EMT in Type II lung epithelial cells [30]. A study by Tanjore et al. demonstrated that one-third of lung fibroblasts that underwent EMT, were derived from Type II lung epithelial cells [31]. Fibroblasts and myofibroblasts are the main cells that synthesize collagen in lung tissues. Microscopic observation of serum-starved NHLF confirmed increased collagen deposition in TGF-β stimulated group (Fig. 5A). Fibers stained with purple (fibrillar collagen) were seen to be increased and less green stains (non-collagenous proteins) were seen compared to control. Results from the quantification studies demonstrated that TGF-β treatment stimulated collagen deposition to 115.5 ± 2.8% as compared to control cells ($p < 0.0001$) (Fig. 5B). Nint and Nint NP displayed collagen reduction in a dose-dependent manner, while nanoparticles consistently displaying better efficacy. Both concentrations of Nint NPs showed significant reduction in collagen deposition compared to TGF-β group (1.25 μM: 101.6 ± 1.1%, 2.5 μM: 98.7 ± 0.9%) ($p < 0.0001$) but no significant difference from control. Nint at both concentrations (1.25 μM: 108.4 ± 2.4%, 2.5 μM: 107.1 ± 1.7%) resulted in statistically higher collagen deposition compared to control ($p < 0.01$ and $p < 0.05$, respectively). Only the highest concentration (2.5 μM) of Nint demonstrated statistical significance against TGF-β group ($p < 0.05$). At 2.5 μM, collagen deposition was significantly reduced for Nint NP compared to Nint treatment ($p < 0.05$) (Fig. 5B).

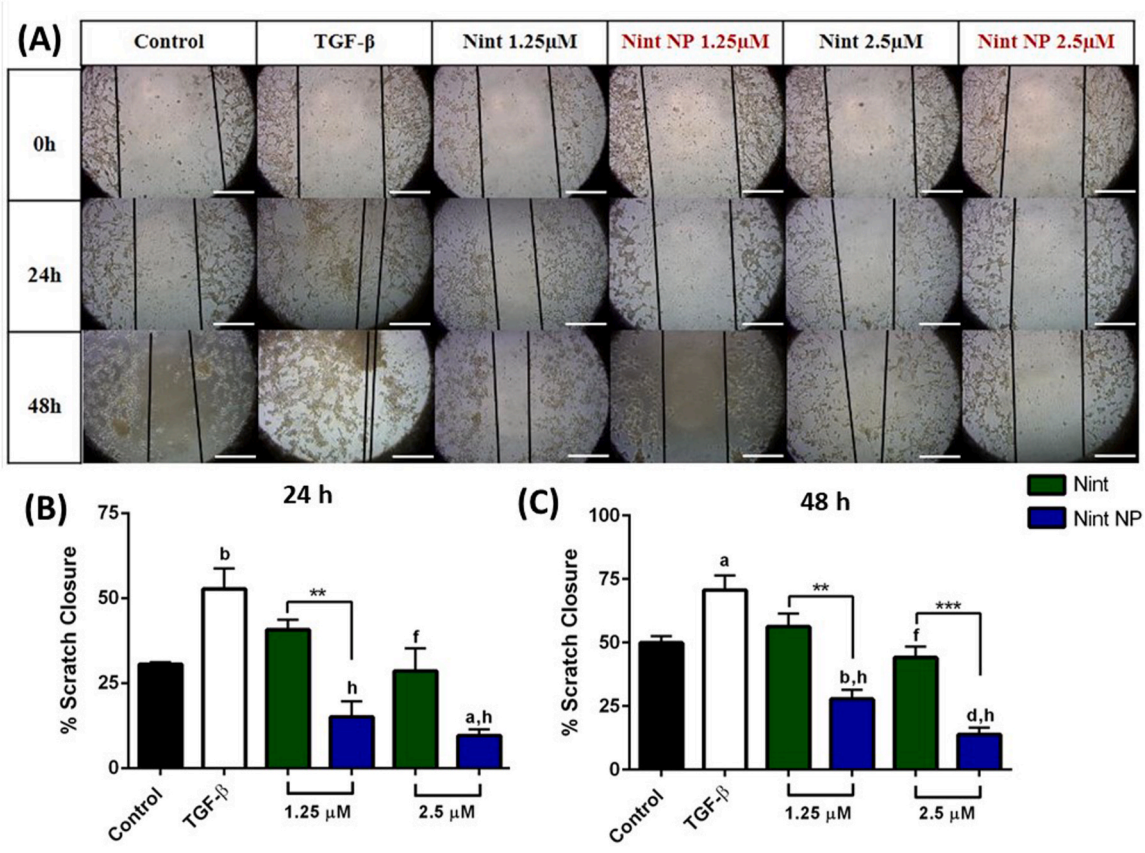

Fig. 4. *In-vitro* wound healing assay with NHLF cells. On confluent serum-starved NHLF cell monolayer, a scratch was created followed by treatment with TGF-β (10 ng/mL) in the presence or absence of Nint and Nint NPs. **A.** Representative images were taken at 10x objective after 24 and 48 h treatment. Cell migration quantification as % scratch closure at **B.** 24 h and **C.** 48 h. $^{**}p < 0.01$ and $^{***}p < 0.001$ comparisons between Nint and Nint NP. $a < 0.05$, $b < 0.01$, and $d < 0.0001$ compared to control. $f < 0.01$ and $h < 0.0001$ compared to TGF-β. Data represent mean ± SEM (n = 3). Scale bar = 500 μm.

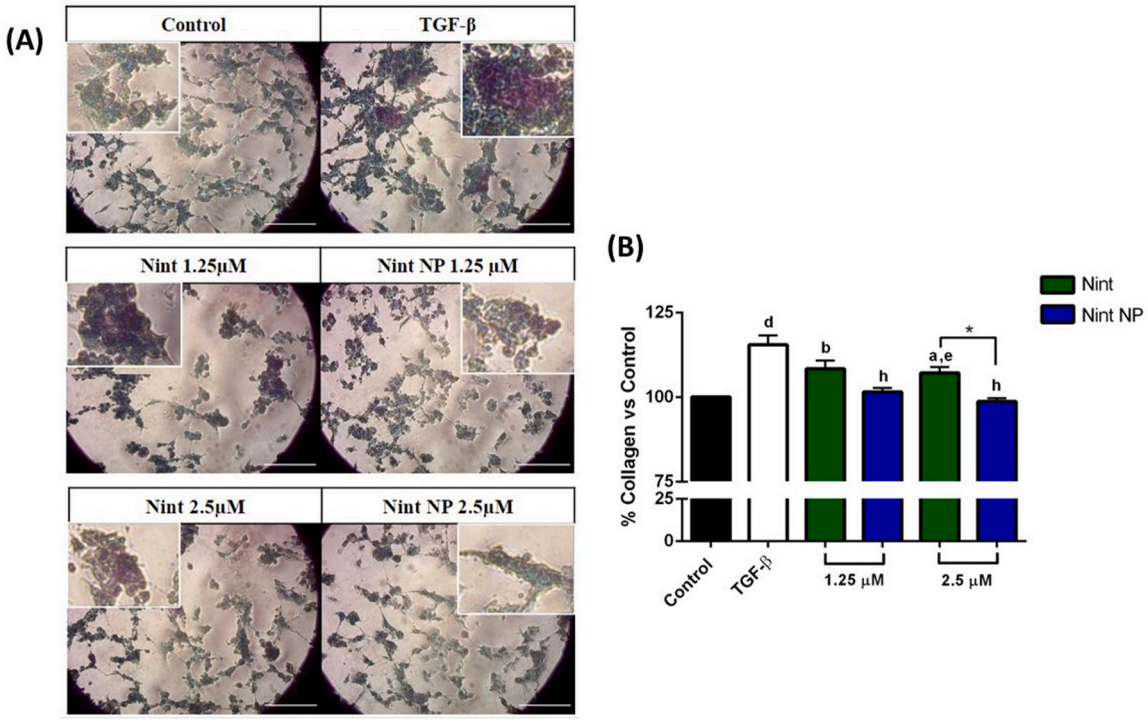

Fig. 5. Effect of Nint and Nint NP on collagen deposition. Serum-starved NHLF cells were stimulated with TGF-β (10 ng/mL), and with Nint or Nint NP. **A.** Representative images showing deposition after Sirius red fast green dye staining. Purple color represent collagen proteins. Scale bar = 100 μm. **B.** Quantification of % collagen content. *$p < 0.05$ comparison between Nint and Nint NP. $a < 0.05$, $b < 0.01$, and $d < 0.0001$ compared to control. $e < 0.05$ and $h < 0.0001$ compared to TGF-β. Data represent mean ± SEM of three separate trials each with n = 3. (For interpretation of the references to color in this figure legend, the reader is referred to the Web version of this article.)

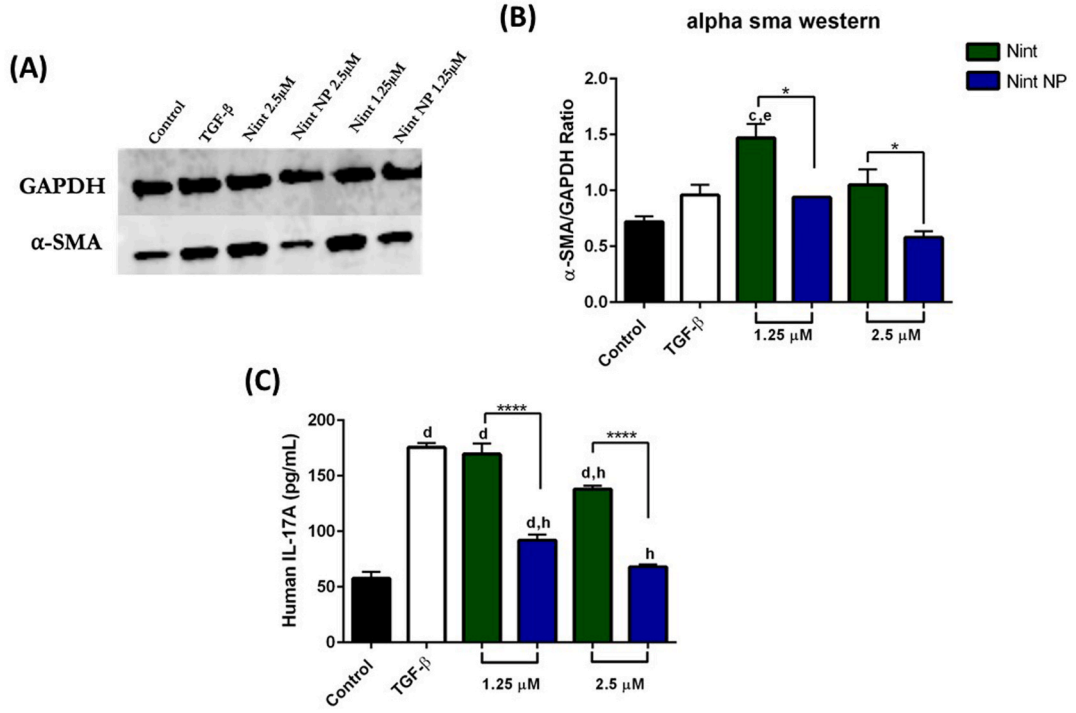

Fig. 6. Western blot analysis of α-SMA in NHLF cells. Serum-starved NHLF cells were stimulated with TGF-β (10 ng/mL), and with Nint or Nint NP. **A.** Representative bands of α-SMA. **B.** Plot represents band intensity ratio for protein and GAPDH in NHLF cells. Data represent mean ± SEM (n = 3). Nint NP effectively decreased inflammatory IL-17A levels and induced autophagy as a separate anti-fibrotic mechanism in NHLF cells. **C.** Quantification of IL-17A levels in media supernatants of NHLF cells using sandwich ELISA method. *$p < 0.05$, ***$p < 0.001$, and **** $p < 0.0001$ comparisons between Nint and Nint NP. b < 0.01, $c < 0.001$, and d < 0.0001 compared to control. $e < 0.05$ and $h < 0.0001$ compared to TGF-β. Data represent mean ± SD (n = 3).

3.7. Effects on α-SMA expression in NHLF cells

α-SMA is a specific marker for fibroblast to myofibroblast differentiation that are responsible for the overproduction of collagen proteins [32]. Western blot analysis demonstrated that TGF-β-stimulated cells resulted in an increase in α-SMA levels (control: 0.72 ± 0.05; TGF-β: 0.96 ± 0.09), though not statistically significant ($p > 0.05$) (Fig. 6A). Both concentrations of Nint NP significantly decreased α-SMA levels compared to free Nint (1.25 μM: Nint: 1.47 ± 0.12, Nint NP: 0.94 ± 0.01) (2.5 μM: Nint: 1.05 ± 0.14, Nint NP: 0.58 ± 0.06) ($p < 0.05$) (Fig. 6B).

3.8. IL-17A levels in TGF-β stimulated NHLF cells

Overexpression or abnormal activity of IL-17 in fibroblasts under pathological conditions can drive IPF pathogenesis [33]. IL-17 or specifically IL-17A levels in cell culture supernatant was measured using a commercially available ELISA assay. As presented in Fig. 6C, marked increased in IL-17A levels were observed in TGF-β group (175.6 ± 3.7 ng/mL) compared to control (57.7 ± 5.9 ng/mL) ($p < 0.0001$). Nint NP (1.25 μM: 92.1 ± 5.1 ng/mL; 2.5 μM: 68.1 ± 1.0 ng/mL) at both concentrations showed significant reduction in IL-17A compared to free Nint (1.25 μM: 169.6 ± 9.7 ng/mL; 2.5 μM: 138.1 ± 3.0 ng/mL) ($p < 0.0001$) and TGF-β group ($p < 0.0001$) (Fig. 6C).

3.9. Effect of Nint and Nint NP on cellular autophagy

There are multiple studies suggesting that the induction of autophagy may have anti-fibrotic effects [34], and Nint has been reported to affect autophagy pathways [35]. Here, an *in-vitro* CYTO-ID® Autophagy Detection assay was used to determine LC3 levels in the treatments, where increased levels indicate induced autophagy. As shown in Fig. S1, the LC3 fluorescent signal upon treatment with TGF-β decreased significantly, 80.6 ± 2.5 % relative to the control cells ($p < 0.01$). There was a dose-dependent increase in LC3 detection in both Nint and Nint NP. Lower concentration (1.25 μM) treatments with Nint and Nint NP did not significantly increase LC3 fluorescence compared to TGF-β group (Nint:87.6 ± 5.4 %; Nint NP: 94.3 ± 1.3%), only the higher concentration (2.5 μM) of Nint NP group (120.6 ± 8.0 %) showed significant increase in LC3 fluorescence ($p < 0.0001$). Statistical significance was observed between Nint and Nint NP at 2.5 μM ($p < 0.001$). Results indicated that 2.5 μM Nint NP significantly induced autophagosome formation in NHLF cells that may impart enhanced anti-fibrotic effects.

3.10. Testing of anti-fibrotic efficacy in a biorelevant in-vitro IPF model

A novel biorelevant *in-vitro* IPF cell model was developed and utilized to better reflect the human IPF disease environment and to better predict treatment efficacy *in-vivo*. A "physiomimetic" approach was utilized that aims to identify and isolate human IPF lung environment in developing disease-specific ECM substrates [26]. Here, diseased lung ECM surface coating was used to coat the cell culture plastics to promote a disease-specific phenotype for the cells to grow in. The Xylyx ECM model acts as a physiologically relevant *in-vitro* model of IPF that could reduce dependence on animal models and accelerate antifibrotic drug screening platforms [26].

3.10.1. Cellular proliferation studies

To test the impact of Nint and Nint NP treatment of cellular hyperproliferation, a hallmark of fibrotic disease development, we performed proliferation studies on NHLF cells grown on IPF lungs-derived extracellular matrix (ECM) coated tissue culture plates. Diseased ECM coating enables the normal NHLF cells to hyper-proliferate in a naturally occurring pathogenic environment [26]. As shown in Fig. 7A. NHLF cells grown in diseased ECM coating conditions, showed significant increase in proliferation as compared to control (137.1 ± 1.0%) ($p < 0.0001$). Nint and Nint NP decreased proliferation in a dose-dependent manner (0.625 μM: Nint: 142.4 ± 1.3%, Nint NP: 120.6 ± 1.9%) (1.25 μM: Nint: 134.5 ± 0.8%, Nint NP: 113.4 ± 0.7%) (2.5 μM: Nint: 111.7 ± 0.3%, Nint NP: 99.1 ± 1.1%). Nint NP consistently showed significant reduction in proliferation compared to free Nint at all concentrations tested (0.625–2.5 μM) ($p < 0.0001$) (Fig. 7A). The only treatment group that showed no significant difference to control or prevented proliferation was Nint NP at the highest concentration of 2.5 μM. Results showed the diseased ECM coating led to NHLF cell proliferation (like TGF-β stimulation) and Nint NP were superior in inhibiting the proliferation.

3.10.2. Human pro-collagen I alpha 1 (COL1A1) ELISA

Collagen production by NHLF cells grown on diseased ECM matrices was analyzed using the ELISA approach. This study specifically quantified the COL1A1 protein in the cell culture supernatants. As seen in Fig. 7B, diseased ECM grown NHLF cells (185.6 ± 0.9 ng/mL) demonstrated significant increase in COL1A1 production compared to control (127.4 ± 3.1 ng/mL) ($p < 0.001$). While both Nint and Nint NP treatments reduced COL1A1 levels in a dose-dependent manner, Nint NPs consistently resulted in significant reduction compared to free Nint ($p < 0.0001$) and diseased control ($p < 0.0001$) (1.25 μM: Nint: 173.3 ± 1.5 ng/mL, Nint NP: 138.7 ± 1.4 ng/mL) (2.5 μM: Nint: 152.4 ± 1.8 ng/mL, Nint NP: 131.2 ± 1.6 ng/mL) (Fig. 7B). Nint NP at 2.5 μM was the only treatment group that showed no significant increase in COL1A1

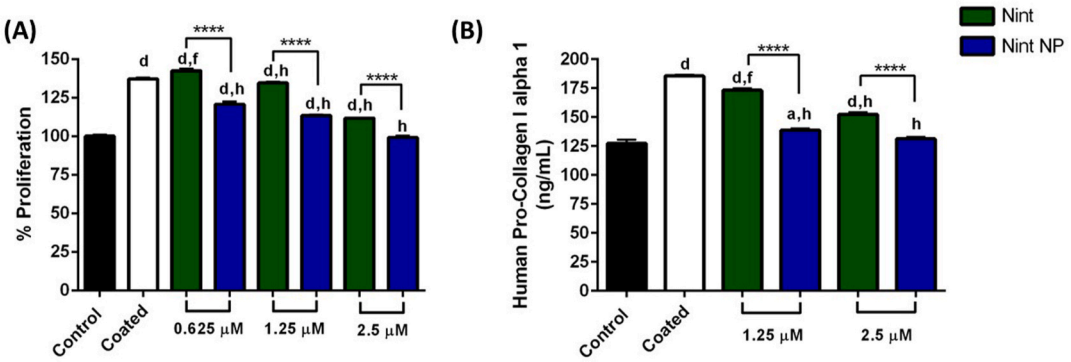

Fig. 7. Xylyx Bio diseased lung ECM coating induced fibrosis in cells. Cell culture plates were coated with diseased substrate prior to seeding the cells. After 24 h serum starvation, cells were treated in the presence or absence of Nint and Nint NPs for 48 h. **A.** Proliferation studies on NHLF cells. Data represent mean ± SEM of three separate trials each with n = 4. **B.** Quantification of human pro-collagen I alpha 1 (COL1A1) level in media supernatants of NHLF cells using ELISA method. Data represent mean ± SEM (n = 6). **** $p < 0.0001$ comparisons between Nint and Nint NP. $a < 0.05$ and $d < 0.0001$ compared to control. $f < 0.01$ and $h < 0.0001$ compared to Coated.

compared to control. Taken together, the diseased surface coating induced fibrotic-related proliferation and collagen production, whereas Nint NPs demonstrated superior anti-fibrotic activities compared to free Nint in this second IPF cell model.

4. Discussion

Nint is a tyrosine kinase inhibitor that exerts anti-inflammatory and anti-fibrotic properties [10]. There have been multiple published reports on the successful encapsulation of Nint in various types of nano-delivery systems, that elucidate the enhanced therapeutic efficacy of the free drug for various cancers and fibrotic lung disease [36–42]. For instance, Singh and Wairkar prepared a promising IPF treatment by incorporating Nint and N-acetyl cysteine (an antioxidant and mucolytic agent) into chitosan nanoparticles that resulted in reduced hydroxyproline content while increasing the antioxidant effects [37]. Separately, Lee et al. fabricated biocompatible aerosolized microgels by incorporating Nint-loaded PLGA NPs and pirfenidone-loaded liposomes. *In-vivo* studies demonstrated prolonged lung retention of the microgels and significant attenuation of IPF progression by promoting TGF-β inhibition and myofibroblast deactivation [43]. Previously, to address shortcomings associated with Nint including low oral bioavailability, low accumulation in the lungs, and high off-target side-effects, we formulated and optimized Nint NPs using a scalable homogenization technology [16]. In this project, we aim to demonstrate the superior anti-fibrotic and anti-inflammatory activities of inhalable Nint-loaded NPs compared to free Nint, as a potential alternative treatment for IPF.

It is well established that nanotechnology is a powerful and customizable tool that can overcome biological and chemical barriers in the human body. However, the production of nanoparticles is a challenging feat, especially in terms of reproducibility of size, monodispersity, and translational scale-up [44]. The limited understanding of scale-up technologies poses significant challenges in effectively bringing nanoparticles to the market at the same rate as their development [45,46]. The Nint NPs developed and tested in this project, is the first Nint-loaded nanoparticle formulation made with scalability in mind, that ensures a seamless transition from small laboratory scale to pilot scale manufacturing [47]. The developed Nint NPs possessed a monodispersed particle size (<200 nm), encapsulated high amounts of Nint, and demonstrated optimal aerodynamic properties for efficient deep-lung deposition, and lung tissue targeting. In a study by Kaur et al., Nint-loaded solid-lipid nanoparticles showed a 2.9-fold increase in oral bioavailability of Nint to Nint control [38]. Whereas, in a study by Ferguson et al., inhaled Nint liposomes showed an 8,000-fold improvement in lung area-under-the-curve (AUC) and lung half-life by 10-fold, compared to oral Nint [42]. These two studies clearly indicate the advantage of locally delivered drug compared to oral administration for improved lung bioavailability. As reported in our recent study, blank NPs revealed good safety profile (>90% cell viability) in normal lung AEC and NHLF cells. Nint NPs also enhance intracellular uptake of therapeutics in AEC and NHLF cells, while avoiding macrophagic uptake [16].

Growth factors, specifically TGF-β-induced epithelial cell proliferation and fibroblast activation, are key events in the pathogenesis of IPF. and the inhibition of TGF-β modulated pathways can alleviate downstream lung injury [48]. Due to activated pathways such as TGF-β, proliferation is elevated in affected lung cells. Therefore, the objective is to suppress such proliferation and fibrotic related pathways to bring the diseased cells back to normal state, where they may maintain normal functions [49]. We performed proliferation testing in 3 different cell lines, A549, AEC, and NHLF cells. A highly proliferative lung-tumor derived A549 cell line has been widely used to represent lung epithelial cells for IPF testing [20,30,50,51]. So, to establish a more accurate IPF cell model, we chose primary AEC and NHLF, derived from healthy human lungs, to induce IPF conditions. From the proliferation studies, Nint NP showed better efficacy compared to Nint, however the results were more significant with A549 cells than with the normal cell lines. The cancerous nature of A549 cells allows them to proliferate rapidly, thus potentially resulting in higher treatment sensitivity [52,53]. Due to loss of cell viability in serum-starved media, the studies with primary cells (AEC and NHLF) were performed only for 48 h, which may be considered a limitation of our study. Research has provided evidence that serum starvation induces apoptosis-mediated cell death in various human cell lines [54–56]. A remedy to improve the study conditions would be to incorporate low levels of serum in the media, consequently, prolonging cell viability and study duration.

EMT is characterized by the loss of cell-cell adhesion and cell junctions, the lack of cell polarity, and the reorganization of actin cytoskeleton [29]. TGF-β is a strong activator of EMT and is considered a key regulator in the process of phenotypic transition. After TGF-β treatment, AEC cells showed characteristic EMT changes from cuboidal to an elongated spindle shape. Interestingly, Nint and Nint NP reduced/-blocked the phenotypic changes, with Nint NPs-treated cells at higher concentration (2.5 μM) completely blocking the transition, thereby preserving the epithelial phenotype. These results corroborated the evaluation of E-cadherin levels, an epithelial marker that is diminished during EMT [57]. E-cadherin is present in the cell membranes of different cells, and induces cell-cell interaction and adhesion [58,59]. Nint treatment has previously been shown to inhibit EMT by regulation of TGF-β/Smad pathways [60]. Our studies demonstrated enhanced efficacy of Nint in halting EMT progression, when encapsulated in nanoparticles. Furthermore, the mesenchymal phenotype is correlated with increased migratory and invasive capabilities [28], which supports our observations from the wound healing assay, where Nint NPs were able to significantly block the migration of cells compared to free Nint. Further, TGF-β activates both Smad and non-Smad signaling pathways. The TGF-β/Smad pathway is activated by the binding of TGF-β to its receptor TβR II, followed by triggering of TβR I, which further pass down the signals to the family of intracellular mediators known as Smads [61]. Non-Smad signaling pathways include PI3K/AKT and MEK/ERK, PI3K/Akt/mTOR, RhoA-ROCK, MAPK/JNK, RAS/PI3K and more pathways to mediate multiple cellular processes such as cell cycle, growth, migration, and immune response [62–64]. Specifically, Nint has been found to inhibit early events in TGF-β signaling involving the phosphorylation of Type II TGF-β receptor, activation of Smad2/3, p38MAPK, ERK1/2, suggesting that the antifibrotic activities of Nint act through both Smad-dependent and Smad-independent signaling pathways of TGF-β [35,65].

The proliferation and differentiation of mesenchymal cells as well as EMT in Type-II epithelial cells lead to the excessive production of fibroblasts and myofibroblasts [30,66]. Fibroblasts and myofibroblasts are responsible for the excessive secretion and deposition of collagen, an ECM component, which destroys the lung architecture and accelerates fibrotic development [67,68]. The present study shows Nint NP exerted superior anti-IPF action by preventing EMT and consequent synthesis of collagen. In keeping with these findings, Murray et al. found increased TGF-β expression is correlated with the increase in pulmonary collagen deposition following intra-tracheal bleomycin exposure [51]. Similarly, Andrade da Silva et al. intratracheally delivered Nint-loaded nanosuspension in lung fibrotic mouse model that provided anti-fibrotic effects (reduced collagen deposition and TGF-β expression) with normalization of lung function at a 100-fold lower dose and 3-fold lower dosing frequency compared to oral Nint group [41]. Furthermore, myofibroblasts that specifically express α-SMA are the main source of collagen production during fibrosis [69]. In this study, Nint NP demonstrated significantly better efficacy than plain Nint in decreasing fibroblast to myofibroblast differentiation by the suppression of α-SMA expression.

IL-17A is an immunologically-mediated inflammatory cytokine that is associated with the progression of IPF [33]. The receptors of IL-17A are ubiquitously expressed in epithelial cells and fibroblasts, which plays an essential role in development of EMT and differentiation into

myofibroblasts, resulting in escalated ECM deposition [70]. Chrysanthopoulou et al. demonstrated that IL-17 production was elevated in fibroblasts following bleomycin challenge, and administration of exogenous IL-17 accelerated fibroblast proliferation, leading to increased expression of α-SMA and collagen [71]. Our study found TGF-β induced the levels of IL-17A in NHLF cells, whereas Nint NPs efficiently reduced the inflammatory response, which corroborated with other observations such as reduced collagen deposition and α-SMA expression. Further, IL-17A neutralization promotes autophagy, which presumably favored collagen resolution in the lung tissues [72]. Autophagy is an adaptive stress response (associated with vacuole formation) that has been reported to be impaired in IPF. Lung tissue from IPF patients and fibroblasts treated with TGF-β demonstrated decreased autophagic activity characterized by decreased LC3B protein expression [73]. In this project, Nint has shown to play anti-fibrotic roles by inhibiting TGF-β signaling, limiting EMT, and downregulating ECM secretion, moreover, Nint can also exert these effects via ATG7-independent autophagy [35]. The present study found Nint NP effectively increased autophagy levels compared to diseased NHLF cells by observing elevated fluorescent levels of LC3.

A significant challenge in the development of effective IPF treatments is the absence of reliable *in-vitro* models that can accurately predict IPF outcomes [74]. An ideal model would emulate human pathophysiology, encompassing the intricate biochemical, structural, and mechanical characteristics of fibrotic lungs. In fibrosis, ECM consists of various fibrogenic growth factors as well as altered structure and other biomechanical compositions compared to normal ECM [75]. Altogether, these matrix remodifications induce a profibrotic environment to activate fibroblasts and other associated cell types. Currently, the most common *in-vitro* IPF drug testing model utilizes TGF-β, but no testing platforms have considered IPF disease-specific ECM components. Therefore, we investigated the feasibility of diseased lung ECM coating developed by Xylyx Bio (Brooklyn, NY, USA) for 2D *in-vitro* model of IPF. The company implemented a physiomimetic approach to develop disease-specific IPF cell culture substrate comprised of lung ECM derived from human IPF tissues [26]. From the results, the diseased coating successfully induced proliferation and collagen type 1 in NHLF cells, thus validating the practicality of this new IPF cell model. Once again, Nint NP displayed superior efficacy in preventing proliferation and collagen production compared to free Nint. Altogether, results from the present study illustrate a definite potential of Nint NPs for the inhalation treatment of IPF.

5. Conclusion

In this project, the FDA-approved IPF medication, nintedanib, was loaded into biodegradable inhaled PLGA nanoparticles using a scalable HPH technique that produced uniformed and reproducible results. *In-vitro* cell culture studies demonstrated that after TGF-β stimulation, Nint NPs not only dramatically prevented changes in cell proliferation, morphology, and migration in pulmonary epithelial cells and fibroblasts, but also inhibited epithelial cell marker (E-cadherin) and prevented fibroblast to myofibroblast marker (α-SMA). Nint NP also proved to be superior in decreasing the ECM deposition during EMT. Moreover, a new IPF cell model was established using Xylyx Bio diseased ECM coating, which was found to prompt proliferation and collagen deposition, while Nint NPs showed superior anti-fibrotic properties. These findings suggest that Nint NPs not only address certain limitations of free Nint such as low aqueous solubility, high oral dose requirements, and oral-associated side effects; but also, are safe for lungs' cellular structure, and are inhalable for better lung tissue deposition. Therefore, inhalable Nint NPs are a promising anti-fibrotic standalone therapy for IPF treatment. The current study lays the groundwork to pursue the development of Nint NPs in preclinical and eventually clinical settings. However, 3D *in-vitro* models on the lung epithelium and preclinical *in-vivo* IPF models need to be tested to further validate the feasibility of Nint NPs as an inhalation therapy of IPF.

Funding

This project was funded with the research funds to VG by College of Pharmacy and Health Sciences, St. John's University, Queens, NY. XW was supported with teaching assistantship by St. John's University. DG was supported by a private industry grant to VG.

CRediT authorship contribution statement

Xuechun Wang: Writing – original draft, Visualization, Validation, Software, Methodology, Investigation, Formal analysis, Data curation, Conceptualization. **Mimansa Goyal:** Methodology, Investigation. **Dnyandev Gadhave:** Writing – review & editing, Methodology. **Vivek Gupta:** Writing – review & editing, Supervision, Resources, Project administration, Methodology, Funding acquisition, Conceptualization.

Declaration of competing interest

The authors declare that they have no known competing financial interests or personal relationships that could have appeared to influence the work reported in this paper.

Data availability

Data will be made available on request.

Appendix A. Supplementary data

Supplementary data to this article can be found online at https://doi.org/10.1016/j.jddst.2024.105615.

References

[1] K.C. Meyer, Pulmonary fibrosis, part I: epidemiology, pathogenesis, and diagnosis, Expet Rev. Respir. Med. (2017) 1–17, https://doi.org/10.1080/17476348.2017.1312346.
[2] Interstitial Lung Disease, in: Pulmonary Fibrosis, 2021. https://www.hopkinsmedicine.org/health/conditions-and-diseases/interstitial-lung-disease-pulmonary-fibrosis. (Accessed 11 January 2023).
[3] Idiopathic pulmonary fibrosis: MedlinePlus Genetics, (n.d.). https://medlineplus.gov/genetics/condition/idiopathic-pulmonary-fibrosis/(accessed January 11, 2023).
[4] IPF, in: Statistics, Facts, and You, Healthline, 2022. https://www.healthline.com/health/managing-idiopathic-pulmonary-fibrosis/ipf-facts. (Accessed 11 January 2023).
[5] M.A. Nieto, R.Y.-J. Huang, R.A. Jackson, J.P. Thiery, EMT: 2016, Cell 166 (2016) 21–45, https://doi.org/10.1016/j.cell.2016.06.028.
[6] J.C. Horowitz, V.J. Thannickal, Epithelial-mesenchymal interactions in pulmonary fibrosis, Semin. Respir. Crit. Care Med. 27 (2006) 600–612, https://doi.org/10.1055/s-2006-957332.
[7] T.A. Mikolasch, H.S. Garthwaite, J.C. Porter, Update in diagnosis and management of interstitial lung disease, Clin. Med. 16 (2016) s71–s78, https://doi.org/10.7861/clinmedicine.16-6-s71.
[8] S.B. Andugulapati, K. Gourishetti, S.K. Tirunavalli, T.B. Shaikh, R. Sistla, Biochanin-A ameliorates pulmonary fibrosis by suppressing the TGF-β mediated EMT, myofibroblasts differentiation and collagen deposition in in vitro and in vivo systems, Phytomedicine 78 (2020) 153298, https://doi.org/10.1016/j.phymed.2020.153298.
[9] M.W. Surber, S. Beck, S. Pham, A.T. Marsden, S.K. Gandi, J. Baily, M.C. McElroy, Inhaled nintedanib is well-tolerated and delivers key pharmacokinetic parameters required to treat bleomycin-induced pulmonary fibrosis, Pulm. Pharmacol. Ther. 63 (2020) 101938, https://doi.org/10.1016/j.pupt.2020.101938.
[10] S. Wind, U. Schmid, M. Freiwald, K. Marzin, R. Lotz, T. Ebner, P. Stopfer, C. Dallinger, Clinical pharmacokinetics and Pharmacodynamics of nintedanib, Clin. Pharmacokinet. 58 (2019) 1131–1147, https://doi.org/10.1007/s40262-019-00766-0.
[11] L. Wollin, E. Wex, A. Pautsch, G. Schnapp, K.E. Hostettler, S. Stowasser, M. Kolb, Mode of action of nintedanib in the treatment of idiopathic pulmonary fibrosis, Eur. Respir. J. 45 (2015) 1434–1445, https://doi.org/10.1183/09031936.00174914.
[12] N.I. Chaudhary, G.J. Roth, F. Hilberg, J. Müller-Quernheim, A. Prasse, G. Zissel, A. Schnapp, J.E. Park, Inhibition of PDGF, VEGF and FGF signalling attenuates

fibrosis, Eur. Respir. J. 29 (2007) 976–985, https://doi.org/10.1183/09031936.00152106.
[13] L. Richeldi, R.M. du Bois, G. Raghu, A. Azuma, K.K. Brown, U. Costabel, V. Cottin, K.R. Flaherty, D.M. Hansell, Y. Inoue, D.S. Kim, M. Kolb, A.G. Nicholson, P. W. Noble, M. Selman, H. Taniguchi, M. Brun, F. Le Maulf, M. Girard, S. Stowasser, R. Schlenker-Herceg, B. Disse, H.R. Collard, Efficacy and safety of nintedanib in idiopathic pulmonary fibrosis, N. Engl. J. Med. 370 (2014) 2071–2082, https://doi.org/10.1056/NEJMoa1402584.
[14] L. Richeldi, U. Costabel, M. Selman, D.S. Kim, D.M. Hansell, A.G. Nicholson, K. K. Brown, K.R. Flaherty, P.W. Noble, G. Raghu, M. Brun, A. Gupta, N. Juhel, M. Klüglich, R.M. du Bois, Efficacy of a tyrosine kinase inhibitor in idiopathic pulmonary fibrosis, N. Engl. J. Med. 365 (2011) 1079–1087, https://doi.org/10.1056/NEJMoa1103690.
[15] G. Epstein-Shochet, S. Pham, S. Beck, S. Naiel, O. Mekhael, S. Revill, A. Hayat, M. Vierhout, B. Bardestein-Wald, D. Shitrit, K. Ask, A.B. Montgomery, M.R. Kolb, M.W. Surber, Inhalation: a means to explore and optimize nintedanib's pharmacokinetic/pharmacodynamic relationship, Pulm, Pharmacol. Ther. 63 (2020) 101933, https://doi.org/10.1016/j.pupt.2020.101933.
[16] X. Wang, D. Gadhave, G. Chauhan, V. Gupta, Development and characterization of inhaled nintedanib-loaded PLGA nanoparticles using scalable high-pressure homogenization technique, J. Drug Deliv. Sci. Technol. (2023) 105233, https://doi.org/10.1016/j.jddst.2023.105233.
[17] R. Iyer, C.C.W. Hsia, K.T. Nguyen, Nano-therapeutics for the lung: state-of-the-Art and future perspectives, Curr. Pharmaceut. Des. 21 (2015) 5233–5244, https://doi.org/10.2174/1381612821666150923095742.
[18] N. Shahabadi, M. Moshiri, A. Roohbakhsh, M. Imenshahidi, M. Hashemi, F. Amin, R. Yazdian-Robati, Z. Salmasi, L. Etemad, A dose-related positive effect of inhaled simvastatin-loaded PLGA nanoparticles on paraquat-induced pulmonary fibrosis in rats, Basic Clin. Pharmacol. Toxicol. (2022), https://doi.org/10.1111/bcpt.13771.
[19] N.S. Kulkarni, V. Parvathaneni, S.K. Shukla, L. Barasa, J.C. Perron, S. Yoganathan, A. Muth, V. Gupta, Tyrosine kinase inhibitor conjugated quantum dots for non-small cell lung cancer (NSCLC) treatment, Eur. J. Pharmaceut. Sci. 133 (2019) 145–159, https://doi.org/10.1016/j.ejps.2019.03.026.
[20] D. Weng, J. Chen, H. Li, F. Liu, L. Zhou, H. Liu, R. Zheng, Y. Jiang, Z. Liu, B. Ge, 2-aminopurine suppresses the TGF-β1-induced epithelial–mesenchymal transition and attenuates bleomycin-induced pulmonary fibrosis, Cell Death Dis. 4 (2018) 1–10, https://doi.org/10.1038/s41420-017-0016-3.
[21] C. Huang, C. Liang, J. Tong, X. Zhong, L. Luo, L. Liang, Y. Wen, L. Zhong, J. Deng, M. Peng, W. Wu, W. Huang, A. Xie, Y. Huang, J. Chen, Soluble E-cadherin participates in BLM-induced pulmonary fibrosis by promoting EMT and lung fibroblast migration, Environ. Toxicol. n/a (n.d.) https://doi.org/10.1002/tox.23986.
[22] C. Hill, M.G. Jones, D.E. Davies, Y. Wang, Epithelial-mesenchymal transition contributes to pulmonary fibrosis via aberrant epithelial/fibroblastic cross-talk, J. Lung Health Dis. 3 (2019) 31–35.
[23] B. Vaidya, S.K. Shukla, S. Kolluru, M. Huen, N. Mulla, N. Mehra, D. Kanabar, S. Palakurthi, S. Ayehunie, A. Muth, V. Gupta, Nintedanib-cyclodextrin complex to improve bio-activity and intestinal permeability, Carbohydr. Polym. 204 (2019) 68–77, https://doi.org/10.1016/j.carbpol.2018.09.080.
[24] N.S. Kulkarni, B. Vaidya, V. Parvathaneni, D. Bhanja, V. Gupta, Repurposing quinacrine for treatment of malignant mesothelioma: in-vitro therapeutic and mechanistic evaluation, Int. J. Mol. Sci. 21 (2020) 6306, https://doi.org/10.3390/ijms21176306.
[25] N.S. Kulkarni, B. Vaidya, V. Parvathaneni, D. Bhanja, V. Gupta, Repurposing quinacrine for treatment of malignant mesothelioma: in-vitro therapeutic and mechanistic evaluation, Int. J. Mol. Sci. 21 (2020) 6306, https://doi.org/10.3390/ijms21176306.
[26] I. Germanguz, E. Aranda, J.C. Xiong, N. Kissel, A. Nichols, E. Gadee, J.D. O'Neill, Fibrotic human lung extracellular matrix as a disease-specific substrate for models of pulmonary fibrosis, J Respir Med Lung Dis 4 (2019).
[27] X. Zhou, J. Wang, J. Chen, Y. Qi, Di Nan, L. Jin, X. Qian, X. Wang, Q. Chen, X. Liu, Y. Xu, Optogenetic control of epithelial-mesenchymal transition in cancer cells, Sci. Rep. 8 (2018) 14098, https://doi.org/10.1038/s41598-018-32539-3.
[28] X. Zhang, Y. Li, Y. Zhang, J. Song, Q. Wang, L. Zheng, D. Liu, Beta-elemene blocks epithelial-mesenchymal transition in human breast cancer cell line MCF-7 through smad3-mediated down-regulation of nuclear transcription factors, PLoS One 8 (2013) e58719, https://doi.org/10.1371/journal.pone.0058719.
[29] F. Liu, Y. Zhou, D. Zhou, M. Kan, X. Niu, Z. Zhang, D. Zhang, L. Tao, L. He, L. Zhan, Y. Liu, Whole DNA methylome profiling in lung cancer cells before and after epithelial-to-mesenchymal transition, Diagn. Pathol. 9 (2014) 66, https://doi.org/10.1186/1746-1596-9-66.
[30] Y. Ji, Y. Dou, Q. Zhao, J. Zhang, Y. Yang, T. Wang, Y. Xia, Y. Dai, Z. Wei, Paeoniflorin suppresses TGF-β mediated epithelial-mesenchymal transition in pulmonary fibrosis through a Smad-dependent pathway, Acta Pharmacol. Sin. 37 (2016) 794–804, https://doi.org/10.1038/aps.2016.36.
[31] H. Tanjore, X.C. Xu, V.V. Polosukhin, A.L. Degryse, B. Li, W. Han, T.P. Sherrill, D. Plieth, E.G. Neilson, T.S. Blackwell, W.E. Lawson, Contribution of epithelial-derived fibroblasts to bleomycin-induced lung fibrosis, Am. J. Respir. Crit. Care Med. 180 (2009) 657–665, https://doi.org/10.1164/rccm.200903-0322OC.
[32] A. Li, X. Xiao, Z.-L. Feng, X. Chen, L.-J. Liu, L.-G. Lin, J.-J. Lu, L.-L. Zhang, Nagilactone D ameliorates experimental pulmonary fibrosis in vitro and in vivo via modulating TGF-β/Smad signaling pathway, Toxicol. Appl. Pharmacol. 389 (2020) 114882, https://doi.org/10.1016/j.taap.2020.114882.
[33] L.J. Celada, J.A. Kropski, J.D. Herazo-Maya, W. Luo, A. Creecy, A.T. Abad, O. S. Chioma, G. Lee, N.E. Hassell, G.I. Shaginurova, Y. Wang, J.E. Johnson, A. Kerrigan, W.R. Mason, R.P. Baughman, G.D. Ayers, G.R. Bernard, D.A. Culver, C. G. Montgomery, T.M. Maher, P.L. Molyneaux, I. Noth, S.E. Mutsaers, C.M. Prele, R. S. Peebles, D.C. Newcomb, N. Kaminski, T.S. Blackwell, L. Van Kaer, W.P. Drake, PD-1 up-regulation on CD4+ T cells promotes pulmonary fibrosis through STAT3-mediated IL-17A and TGF-β1 production, Sci. Transl. Med. 10 (2018) eaar8356, https://doi.org/10.1126/scitranslmed.aar8356.
[34] S. Liao, P. Sun, Y. Gu, X. Rao, L. Zhang, Y. Ou-Yang, Autophagy and pulmonary disease, Ther. Adv. Respir. Dis. 13 (2019) 1753466619890538, https://doi.org/10.1177/1753466619890538.
[35] S. Rangarajan, A. Kurundkar, D. Kurundkar, K. Bernard, Y.Y. Sanders, Q. Ding, V. B. Antony, J. Zhang, J. Zmijewski, V.J. Thannickal, Novel mechanisms for the antifibrotic action of nintedanib, Am. J. Respir. Cell Mol. Biol. 54 (2016) 51–59, https://doi.org/10.1165/rcmb.2014-0445OC.
[36] Y. Xu, Y. Liu, T. He, Y. Zhang, M. Wang, H. Yuan, M. Yang, Biguanides decorated albumin nanoparticles loading nintedanib for synergic enhanced hepatocellular carcinoma therapy, Colloids Surf. B Biointerfaces 207 (2021) 112020, https://doi.org/10.1016/j.colsurfb.2021.112020.
[37] S. Singh, S. Wairkar, Long-circulating thiolated chitosan nanoparticles of nintedanib with N-acetyl cysteine for treating idiopathic pulmonary fibrosis: in vitro assessment of cytotoxicity, antioxidant, and antifibrotic potential, Int. J. Pharm. 644 (2023) 123322, https://doi.org/10.1016/j.ijpharm.2023.123322.
[38] R. Kaur, T.B. Shaikh, H. Priya Sripadi, M. Kuncha, U.V.R. Vijaya Sarathi, H. Kulhari, S. Balaji Andugulapati, R. Sistla, Nintedanib solid lipid nanoparticles improve oral bioavailability and ameliorate pulmonary fibrosis in vitro and in vivo models, Int. J. Pharm. (2023) 123644, https://doi.org/10.1016/j.ijpharm.2023.123644.
[39] D. Li, A. Zhao, J. Zhu, C. Wang, J. Shen, Z. Zheng, F. Pan, Z. Liu, Q. Chen, Y. Yang, Inhaled lipid nanoparticles alleviate established pulmonary fibrosis, Small 19 (2023) 2300545, https://doi.org/10.1002/smll.202300545.
[40] S.K. Shukla, V. Nguyen, M. Goyal, V. Gupta, Cationically modified inhalable nintedanib niosomes: enhancing therapeutic activity against non-small-cell lung cancer, Nanomed 17 (2022) 935–958, https://doi.org/10.2217/nnm-2022-0045.
[41] L.H. Andrade da Silva, J.B. Vieira, M.R. Cabral, M.A. Antunes, D. Lee, F.F. Cruz, J. Hanes, P.R.M. Rocco, M.M. Morales, J.S. Suk, Development of nintedanib nanosuspension for inhaled treatment of experimental silicosis, Bioeng. Transl. Med. 8 (2022) e10401, https://doi.org/10.1002/btm2.10401.
[42] L.T. Ferguson, X. Ma, J.W. Myerson, J. Wu, P.M. Glassman, M.E. Zamora, E. D. Hood, M. Zaleski, M. Shen, E.-O. Essien, V.V. Shuvaev, J.S. Brenner, Mechanisms by which liposomes improve inhaled drug delivery for alveolar diseases, Adv. Nanobiomed Res. 3 (2023) 2200106, https://doi.org/10.1002/anbr.202200106.
[43] W.T. Lee, H. Lee, J. Kim, Y. Jung, E. Choi, J.H. Jeong, J.-H. Jeong, J.H. Lee, Y. S. Youn, Alveolar macrophage phagocytosis-evading inhaled microgels incorporating nintedanib-PLGA nanoparticles and pirfenidone-liposomes for improved treatment of pulmonary fibrosis, Bioact. Mater. 33 (2024) 262–278, https://doi.org/10.1016/j.bioactmat.2023.11.005.
[44] J.K. Patel, Y. Pathak (Eds.), Emerging Technologies for Nanoparticle Manufacturing, Springer, Cham, 2021.
[45] R. Paliwal, R.J. Babu, S. Palakurthi, Nanomedicine scale-up technologies: feasibilities and challenges, AAPS PharmSciTech 15 (2014) 1527–1534, https://doi.org/10.1208/s12249-014-0177-9.
[46] M.S. Muthu, B. Wilson, Challenges posed by the scale-up of nanomedicines, Nanomed 7 (2012) 307–309, https://doi.org/10.2217/nnm.12.3.
[47] V. Parvathaneni, in: EXPLORING EFFICACY OF AN AN ANTI-MALARIAL NANOMEDICINE IN NON-SMALL CELL LUNG CANCER TREATMENT, 2021. St. John's University, https://scholar.stjohns.edu/cgi/viewcontent.cgi?article=1192&context=theses_dissertations. (Accessed 14 January 2023).
[48] L. Li, D. Li, L. Xu, P. Zhao, Z. Deng, X. Mo, P. Li, L. Qi, J. Li, J. Gao, Total extract of Yupingfeng attenuates bleomycin-induced pulmonary fibrosis in rats, Phytomedicine 22 (2015) 111–119, https://doi.org/10.1016/j.phymed.2014.10.011.
[49] L. Tao, J. Cao, W. Wei, H. Xie, M. Zhang, C. Zhang, Protective role of rhapontin in experimental pulmonary fibrosis in vitro and in vivo, Int. Immunopharm. 47 (2017) 38–46, https://doi.org/10.1016/j.intimp.2017.03.020.
[50] L. Shi, N. Dong, X. Fang, X. Wang, Regulatory mechanisms of TGF-β1-induced fibrogenesis of human alveolar epithelial cells, J. Cell Mol. Med. 20 (2016) 2183–2193, https://doi.org/10.1111/jcmm.12918.
[51] L. Murray, T.-L. Hackett, S. Warner, F. Shaheen, R. Argentieri, P. Dudas, F. Farrell, BMP-7 does not protect against bleomycin-induced lung or skin fibrosis, PLoS One 3 (2008) e4039, https://doi.org/10.1371/journal.pone.0004039.
[52] M. Carter, J.C. Shieh, Chapter 13 - cell culture techniques, in: M. Carter, J.C. Shieh (Eds.), Guide Res. Tech. Neurosci., Academic Press, New York, 2010, pp. 281–296, https://doi.org/10.1016/B978-0-12-374849-2.00013-6.
[53] M. Carter, J. Shieh, Chapter 14 - cell culture techniques, in: M. Carter, J. Shieh (Eds.), Guide Res. Tech. Neurosci, Academic Press, San Diego, 2015, pp. 295–310, https://doi.org/10.1016/B978-0-12-800511-8.00014-9. Second Ed.
[54] F. Braun, J. Bertin-Ciftci, A.-S. Gallouet, J. Millour, P. Juin, Serum-nutrient starvation induces cell death mediated by bax and puma that is counteracted by p21 and unmasked by bcl-xL inhibition, PLoS One 6 (2011) e23577, https://doi.org/10.1371/journal.pone.0023577.
[55] Y. Huang, Z. Fu, W. Dong, Z. Zhang, J. Mu, J. Zhang, Serum starvation-induces down-regulation of Bcl-2/Bax confers apoptosis in tongue coating-related cells in vitro, Mol. Med. Rep. 17 (2018) 5057–5064, https://doi.org/10.3892/mmr.2018.8512.
[56] M. Rashid, K.M. Coombs, Serum-reduced media impacts on cell viability and protein expression in human lung epithelial cells, J. Cell. Physiol. 234 (2019) 7718–7724, https://doi.org/10.1002/jcp.27890.

[57] R. Kalluri, R.A. Weinberg, The basics of epithelial-mesenchymal transition, J. Clin. Invest. 119 (2009) 1420–1428, https://doi.org/10.1172/JCI39104.
[58] P.J. Marie, E. Haÿ, D. Modrowski, L. Revollo, G. Mbalaviele, R. Civitelli, Cadherin-mediated cell-cell adhesion and signaling in the skeleton, Calcif. Tissue Int. 94 (2014) 46–54, https://doi.org/10.1007/s00223-013-9733-7.
[59] U. Tepass, K. Truong, D. Godt, M. Ikura, M. Peifer, Cadherins in embryonic and neural morphogenesis, Nat. Rev. Mol. Cell Biol. 1 (2000) 91–100, https://doi.org/10.1038/35040042.
[60] H. Ihara, Y. Mitsuishi, M. Kato, F. Takahashi, K. Tajima, T. Hayashi, M. Hidayat, W. Winardi, A. Wirawan, D. Hayakawa, K. Kanamori, N. Matsumoto, T. Yae, T. Sato, S. Sasaki, K. Takamochi, Y. Suehara, D. Ogura, S. Niwa, K. Suzuki, K. Takahashi, Nintedanib inhibits epithelial-mesenchymal transition in A549 alveolar epithelial cells through regulation of the TGF-β/Smad pathway, Respir. Investig. 58 (2020) 275–284, https://doi.org/10.1016/j.resinv.2020.01.003.
[61] X. Zhang, K.-W. Min, J. Liggett, S.J. Baek, Disruption of the transforming growth factor-β pathway by tolfenamic acid via the ERK MAP kinase pathway, Carcinogenesis 34 (2013) 2900–2907, https://doi.org/10.1093/carcin/bgt250.
[62] X. Feng, W. Feng, Y. Ji, T. Jin, J. Li, J. Guo, Transforming growth factor-β1 negatively regulates SOCS7 via EGR1 during wound healing, Cell Commun, Signal. 20 (2022) 86, https://doi.org/10.1186/s12964-022-00893-5.
[63] S. Lamouille, R. Derynck, Cell size and invasion in TGF-beta-induced epithelial to mesenchymal transition is regulated by activation of the mTOR pathway, J. Cell Biol. 178 (2007) 437–451, https://doi.org/10.1083/jcb.200611146.
[64] J. Wang, H. Xiang, Y. Lu, T. Wu, Role and clinical significance of TGF-β1 and TGF-βR1 in malignant tumors, Int. J. Mol. Med. 47 (2021) 1, https://doi.org/10.3892/ijmm.2021.4888, submitted for publication.
[65] X. Lin, J. Wen, R. Liu, W. Gao, B. Qu, M. Yu, Nintedanib inhibits TGF-β-induced myofibroblast transdifferentiation in human Tenon's fibroblasts, Mol. Vis. 24 (2018) 789–800.
[66] B.C. Willis, R.M. duBois, Z. Borok, Epithelial origin of myofibroblasts during fibrosis in the lung, Proc. Am. Thorac. Soc. 3 (2006) 377–382, https://doi.org/10.1513/pats.200601-004TK.
[67] E. Crouch, Pathobiology of pulmonary fibrosis, Am. J. Physiol. 259 (1990) L159–L184, https://doi.org/10.1152/ajplung.1990.259.4.L159.
[68] G. Raghu, L.J. Striker, L.D. Hudson, G.E. Striker, Extracellular matrix in normal and fibrotic human lungs, Am. Rev. Respir. Dis. 131 (1985) 281–289, https://doi.org/10.1164/arrd.1985.131.2.281.
[69] G. Gabbiani, The biology of the myofibroblast, Kidney Int. 41 (1992) 530–532, https://doi.org/10.1038/ki.1992.75.
[70] T. Wang, Y. Liu, J.-F. Zou, Z.-S. Cheng, Interleukin-17 induces human alveolar epithelial to mesenchymal cell transition via the TGF-β1 mediated Smad2/3 and ERK1/2 activation, PLoS One 12 (2017) e0183972, https://doi.org/10.1371/journal.pone.0183972.
[71] A. Chrysanthopoulou, I. Mitroulis, E. Apostolidou, S. Arelaki, D. Mikroulis, T. Konstantinidis, E. Sivridis, M. Koffa, A. Giatromanolaki, D.T. Boumpas, K. Ritis, K. Kambas, Neutrophil extracellular traps promote differentiation and function of fibroblasts, J. Pathol. 233 (2014) 294–307, https://doi.org/10.1002/path.4359.
[72] H. Liu, S. Mi, Z. Li, F. Hua, Z.-W. Hu, Interleukin 17A inhibits autophagy through activation of PIK3CA to interrupt the GSK3B-mediated degradation of BCL2 in lung epithelial cells, Autophagy 9 (2013) 730–742, https://doi.org/10.4161/auto.24039.
[73] J. Araya, J. Kojima, N. Takasaka, S. Ito, S. Fujii, H. Hara, H. Yanagisawa, K. Kobayashi, C. Tsurushige, M. Kawaishi, N. Kamiya, J. Hirano, M. Odaka, T. Morikawa, S.L. Nishimura, Y. Kawabata, H. Hano, K. Nakayama, K. Kuwano, Insufficient autophagy in idiopathic pulmonary fibrosis, Am. J. Physiol. Lung Cell Mol. Physiol. 304 (2013) L56–L69, https://doi.org/10.1152/ajplung.00213.2012.
[74] J.E. Nichols, J.A. Niles, S.P. Vega, J. Cortiella, Novel in vitro respiratory models to study lung development, physiology, pathology and toxicology, Stem Cell Res. Ther. 4 (Suppl 1) (2013) S7, https://doi.org/10.1186/scrt368.
[75] J.H. Kristensen, M.A. Karsdal, F. Genovese, S. Johnson, B. Svensson, S. Jacobsen, P. Hägglund, D.J. Leeming, The role of extracellular matrix quality in pulmonary fibrosis, Respir. Int. Rev. Thorac. Dis. 88 (2014) 487–499, https://doi.org/10.1159/000368163.